Measurement of sound power and absorption in reverberation chambers using energy density

David B. Nutter,[a] Timothy W. Leishman, Scott D. Sommerfeldt, and Jonathan D. Blotter
Acoustics Research Group, Department of Physics and Astronomy, Department of Mechanical Engineering, Brigham Young University, Provo, Utah 84602

(Received 2 October 2006; revised 1 February 2007; accepted 5 February 2007)

Reverberation chamber measurements typically rely upon spatially averaged squared pressure for the calculation of sound absorption, sound power, and other acoustic values. While a reverberation chamber can provide an approximately diffuse sound field, variations in sound pressure consistently produce uncertainty in measurement results. This paper explores the benefits of using total energy density or squared particle velocity magnitude (kinetic energy density) instead of squared pressure (potential energy density) for sound absorption and sound power measurements. The approaches are based on methods outlined in current ISO standards. The standards require a sufficient number of source-receiver locations to obtain suitable measurement results. The total and kinetic energy densities exhibit greater spatial uniformity at most frequencies than potential energy density, thus requiring fewer source-receiver positions to produce effective results. Because the total energy density is typically the most uniform of the three quantities at low frequencies, its use could also impact the usable low-frequency ranges of reverberation chambers. In order to employ total and kinetic energy densities for sound absorption measurements, relevant energy-based impulse responses were developed as part of the work for the assessment of sound field decays.
 [DOI: 10.1121/1.2713667]

PACS number(s): 43.55.Nd, 43.55.Ev, 43.50.Cb [AJZ] Pages: 2700–2710

I. INTRODUCTION

Current ISO standards governing the measurement of sound power and sound absorption in reverberation chambers rely upon the measurement of spatially averaged squared pressure. The squared pressure at a single point in a chamber is proportional to the potential energy density at that point, representing only a portion of the available energetic information. In 1974, Tichy and Baade suggested that total energy density might be used more efficiently for the determination of sound power, with the expectation that it would have less spatial variation over chamber sound fields.[1] The same year, Cook and Schade used a limited theoretical analysis to conclude that the spatial variance (apparently the normalized spatial standard deviation) of total energy density in a reverberation chamber should be approximately one-half that of potential energy density.[2] They reported experimental results from plane-wave tube measurements and surmized that the spatial variance of total energy density should generally be much less than that of either potential or kinetic energy density. Sepmeyer and Walker described preliminary measurements of total energy density in a reverberation room, confirming that its variation was roughly one-half that of squared pressure.[3] In 1976, Waterhouse and Cook investigated the spatial dependence of the potential, kinetic, and total energy densities for axial, tangential, and oblique modes in reverberation rooms.[4] This extended earlier descriptions of their behaviors in the vicinities of reflecting boundaries.[5,6]

In 1979, Jacobsen used a stochastic diffuse field model with analytical and statistical arguments to show that the normalized spatial variance of the mean-square pressure in a reverberant field should be one.[7] He verified this experimentally for frequencies above the Schroeder cutoff frequency. He then derived the normalized variance for the mean-square value of each Cartesian particle velocity component, finding that they were likewise one, whereas that of the resultant mean-square particle velocity was $\frac{1}{3}$. The normalized variances of the potential, kinetic, and total energy densities were 1, $\frac{1}{3}$, and $\frac{1}{3}$, leading to normalized spatial standard deviations of 1, 0.58, and 0.58, respectively. In 1987, Moryl and Hixson also explored the spatial distribution of the energy densities in reverberation rooms.[8,9] For several pure-tone excitations and a linear traverse in the central region of a reverberation room, they found normalized spatial standard deviations that were 0.94, 0.61, and 0.64, respectively, close to Jacobsen's broader field predictions.

While not directly related to reverberation chamber measurements, several other successful applications of total energy density have been described more recently. One application, originally pursued in three-dimensional enclosures by Parkins *et al.*, used energy density to increase the global extent of active noise control.[10] Their work focused on fields with low modal density. In another application, Bonsi *et al.* proposed a "quadraphonic impulse response" for acoustical enhancement of audio.[11] While this latter work was not known to the authors during the time of research, it is essentially the "energy density impulse response" derived herein for certain reverberation chamber measurements.

Despite the importance of these earlier studies, the use of total energy density for sound power and sound absorption

[a]Current affiliation: SARA, Inc., 6300 Gateway Dr., Cypress, CA 90630-4844.

measurements in reverberation chambers has required further development. Because no reliable method was widely available to assess kinetic and total energy densities during the developmental stages of these measurements, spatially averaged squared pressure was accepted for the applications and continues to be used to this day. Nevertheless, recent developments encourage further exploration of the topic.

In very early research during the 1930s, Wolff and Massa used a pressure gradient microphone to estimate particle velocity and compared variations of potential, kinetic, and total energy density in a room.[12] Since that time, several improved methods have been introduced to estimate particle velocity, allowing kinetic and total energy densities to be measured with greater accuracy and consistency.[13–16] The introduction of the Microflown™ sensor, a micromachined device that more directly measures particle velocity, has provided additional means to measure energy density up to 20 kHz.[17,18]

With such feasible measurement options now available, one would anticipate that the suggestion given by Tichy and Baade would be revisited. This was a primary focus of the research reported in this paper. It presents an exploration of their assertion for sound power measurements, while extending the concept through the use of kinetic energy density (or squared particle velocity magnitude) alone. It also explores the use of kinetic and total energy densities for sound absorption measurements. In all cases, it does so by introducing measurement procedures analogous to those found in existing ISO standards (ISO 3741 and 354).[19,20]

Many concerns about sound power measurements in reverberant rooms have been expressed in the past. They address specific problems with the underestimation of sound power at lower frequencies, changes in radiation impedance seen by the sound source, insufficient sound field sampling, and reproducibility at different source positions.[19] The Waterhouse correction is applied to measurements taken in the diffuse field to account for the potential energy stored in interference patterns near reflecting surfaces.[5] Schaffner modified the correction to include absorption effects of the boundaries.[21] Another correction was introduced by Vorländer to account for "missing sound level" using diffuse field equations.[22] Changes in radiation impedance are due to reflections from nearby surfaces and atmospheric conditions. The use of stationary diffusers, a large room volume, and low-frequency absorption can reduce some effects of reflections. A rotating diffuser can also improve spatial averaging of the sound field, which reduces the number of receiver positions required for adequate sampling.[1] Averaging over several source positions may likewise reduce variation effects. Acceptable standard deviation values are outlined in the ISO standards 3741 and 354, and are based on models of statistical distribution of the squared pressure for high modal densities.[23,24]

Reverberation time (T_{60}) measurements used to assess sound absorption also vary with position in a reverberation chamber.[25] Hodgson suggested that exponential decay, while predicted by the Eyring equation[26] for a diffuse field, depends on room shape, room absorption, and the absorption of sound diffusers.[27] Sound may become "trapped" in certain regions of a room, resulting in decays that deviate from theoretical predictions.[28] In practice, the T_{60} may be obtained at a given point by performing backward (Schroeder) integration of the squared-pressure impulse response[29] or by assessing the decay rate after a source producing a steady-state sound field has been turned off. Both the integrated impulse response method and the decay curve method are allowed by ISO 354.

Several interrelated questions served as motivations for the research reported in this paper. First, is it possible to extend the usable low-frequency range of an existing chamber without adding measurement positions or absorption to increase modal overlap? If so, reverberation chambers could service several types of measurements with fewer required modifications. Second, could smaller reverberant rooms that fail to meet volume requirements or other rooms that otherwise fail to satisfy qualification standards be used to obtain reliable measurement results, thus enhancing means for those without access to ideal facilities? Third, if measurements were taken of an acoustic field quantity with greater spatial uniformity than squared pressure, how would this reduce the required number of measurement positions in a given chamber? Fourth, could currently allowed deviation values for reverberation chamber measurements be substantially reduced through alternative field measurements? The research was undertaken to address these questions through specific exploration of kinetic and total energy densities in reverberant rooms.[30] While the work involved some theoretical and numerical modeling, it primarily involved experimental efforts.

The following sections address pertinent concepts of the energy density methods and calculations required to evaluate sound absorption and sound power in reverberation chambers. They include derivations of pertinent energy-based impulse responses. Experimental results for two chambers are presented, along with further discussion of the measurement implications.

II. METHODS

Sound absorption and sound power measurements were taken in two rooms. The first was a qualified reverberation chamber with dimensions of $4.96\text{m} \times 5.89\text{m} \times 6.98\text{m}$, a volume of approximately 204 m^3, and a Schroeder frequency of 410 Hz (with no low-frequency absorption in place). The second was a much smaller chamber with dimensions of $5.70\text{m} \times 4.30\text{m} \times 2.50\text{m}$, a volume of approximately 61 m^3, and a Schroeder frequency of 552 Hz (with no low-frequency absorption in place). Both chambers incorporated stationary diffusers that were consistently used throughout the investigation. Because the volume of the smaller chamber did not meet qualification standards, its conventional low-frequency measurements were expected to suffer in accuracy.

A Microflown™ sensor, consisting of one acoustic pressure sensor and three orthogonal particle velocity sensors for each Cartesian component, was used to measure the chamber sound fields at discrete points. The output signal of each transducer was fed to a signal conditioning box. The corresponding outputs of the box were then fed to a control room

for digitization, analysis, storage, and later processing. A dodecahedron loudspeaker was used as a source to assess the sound absorption of test specimens. A TEF 20 analyzer drove the loudspeaker amplifier with a maximum-length sequence and sequentially monitored each output channel of the sensor to assess the associated room impulse responses for the selected source-receiver locations. A Matlab routine was developed to compute the Schroeder decay curves using the integrated impulse response method. A Sony DAT recorder was used to record the steady-state responses from a Brüel & Kjær reference sound source for sound power measurements. These measurements were processed using another Matlab routine. In all cases, the temperature, relative humidity, and barometric pressure of the chambers were monitored at positions close to the sensor. The following sections provide additional details about the specific methods used for the sound absorption and sound power measurements.

A. Sound absorption

1. Standard formulation for equivalent absorption area

From ISO 354, the equivalent sound absorption area of a test specimen for a given frequency band is

$$A_T = 55.3V\left(\frac{1}{c_2T_2} - \frac{1}{c_1T_1}\right) - 4V(m_2 - m_1), \tag{1}$$

where T denotes the arithmetic mean value of T_{60}, c is the speed of sound, V is the room volume, and m is the power attenuation coefficient. The subscripts 1 and 2 refer to values of the chamber when empty and with the test specimen present, respectively. The value for m can be obtained from the relationship

$$m = \frac{\alpha}{10\log(e)}, \tag{2}$$

where α is the pure-tone sound-attenuation coefficient for atmospheric absorption, in decibels per meter. This coefficient is obtained by inserting the values of temperature, relative humidity, and barometric pressure into equations detailed in ISO 9613.[31] The accuracy of the pure-tone attenuation coefficient is estimated to be ±10% under recommended atmospheric measurement conditions.[20] This has strong effects on measurements at higher frequencies, as will be discussed later.

For this research, two different types of samples were measured. The first was a planar 5-cm-thick semi-rigid fiberglass insulation panel resting on the floor with an A-mounting (see ISO 354). The total exposed surface area of the material, including edges, was 10.65 m^2 for the large chamber and 6.11 m^2 for the small chamber. The second sample consisted of three upholstered office chairs. The results for the latter are presented elsewhere.[30]

2. Use of alternate impulse responses

The behavior of a linear time-invariant system may be characterized by its impulse response $h(t)$, defined as the time-domain output of the system due to the application of a unit impulse function (Dirac delta function) $\delta(t)$ at the input, a time τ beforehand. For an arbitrary input function $a(t)$, the output $b(t)$ is given by the convolution integral

$$b(t) = \int_{-\infty}^{\infty} h(\tau)a(t-\tau)d\tau, \tag{3}$$

such that if $a(t) = \delta(t)$,

$$b(t) = \int_{-\infty}^{\infty} h(\tau)\delta(t-\tau)d\tau = h(t). \tag{4}$$

In an enclosed sound field, the impulse response $h_p(\tau)$ between a source and a receiver is typically considered in terms of the acoustic pressure $p(t)$ at the receiver "output" position. However, the individual Cartesian components of the particle velocity [$u_x(t)$, $u_y(t)$, and $u_z(t)$] also satisfy the linear wave equation[32] and can therefore be used for the definition of additional impulse responses. For the x component of the particle velocity, the convolution integral becomes

$$u_x(t) = \int_{-\infty}^{\infty} h_{u_x}(\tau)a(t-\tau)d\tau, \tag{5}$$

where the impulse response $h_{u_x}(\tau)$ is defined by the application of the unit impulse:

$$u_x(t) = \int_{-\infty}^{\infty} h_{u_x}(\tau)\delta(t-\tau)d\tau = h_{u_x}(t). \tag{6}$$

Similar relationships follow for the y and z components of the particle velocity. Since the square of the vector particle velocity magnitude is defined as

$$u^2(t) = |\mathbf{u}(t)|^2 = u_x^2(t) + u_y^2(t) + u_z^2(t), \tag{7}$$

one can analogously define a squared impulse response for the vector particle velocity magnitude:

$$h_u^2(t) = h_{u_x}^2(t) + h_{u_y}^2(t) + h_{u_z}^2(t). \tag{8}$$

An impulse response $h_w(\tau)$ associated with total energy density then follows with appropriate weightings:

$$h_w(t) = \frac{1}{2\rho_0 c^2}h_p^2(t) + \frac{\rho_0}{2}h_u^2(t). \tag{9}$$

To study the impact of each specified measurements, the impulse responses obtained in Eqs. (8) and (9) can be used in calculations in place of $h_p^2(t)$.

Because absorption data are typically observed in one-third-octave frequency bands, the primary impulse responses are filtered before they are squared in order to preserve spectral information. Figure 1 shows examples of squared pressure, squared velocity magnitude, and total energy density impulse responses in the 250-Hz one-third-octave band at one position in the larger chamber. The impulse responses are displayed on logarithmic amplitude scales. Of practical concern is the error introduced through the factors ρ_0 and c. In many cases, the relative amplitude of the squared impulse response is not important, since T_{60} is merely derived from the slope of the integration curve. However, the combination of several impulse responses weighted by these constants suggests that errors of the measured atmospheric values

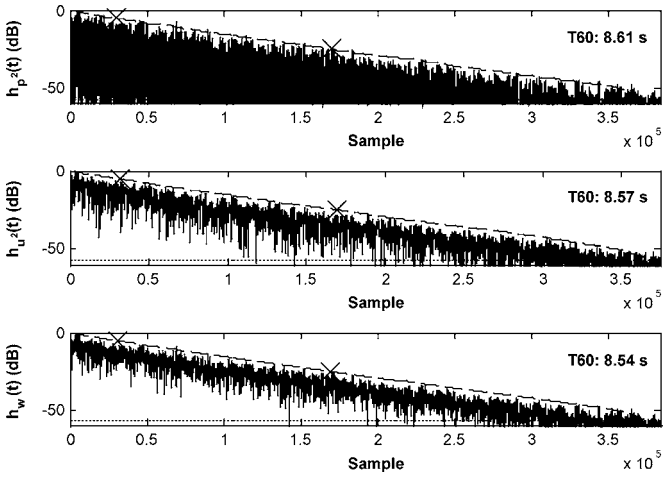

FIG. 1. Impulse responses of pressure, particle velocity magnitude, and total energy density in the 250-Hz one-third-octave band, obtained at one position in the large chamber. The abscissa corresponds to the sample number for a 48 kHz sampling frequency. The dashed line is the Schroeder integration curve. The horizontal dotted line shows the noise floor. The integration starts where this line intersects with the Schroeder curve. The cross marks show the −5 and −25 dB down points.

could lead to errors in the total energy density impulse response. The significance of these errors will be treated in a later section.

B. Sound power

1. Standard formulation using sound pressure

The sound pressure level (SPL or L_p) at a point in a chamber is given by

$$L_p = 10 \log\left(\frac{p_{\mathrm{rms}}^2}{p_{\mathrm{ref}}^2}\right), \tag{10}$$

where p_{rms} is the measured rms acoustic pressure and p_{ref} is the reference acoustic pressure (20 μPa). Following procedures given in ISO 3741, the sound power level (PWL or L_W) of a source under test is given by

$$L_W = \bar{L}_p + \left[10 \log \frac{A}{A_0} + 4.34 \frac{A}{S} + 10 \log\left(1 + \frac{Sc}{8Vf}\right) - 25 \log\left(\frac{427}{400}\sqrt{\frac{273}{273 + T_c}}\frac{B}{B_0}\right) - 6 \right], \tag{11}$$

where $\bar{L}_p$ is the SPL in a given frequency band, averaged over all source and microphone positions, A is the equivalent sound absorption area in the test room, A_0 is 1 m^2, S is the total surface area of all room surfaces in m^2,[33] V is the room volume in m^3, f is the mid-band frequency of the measurement in Hz, c is the speed of sound in m/s at temperature T_c (in °C), B is the atmospheric pressure in Pa, and B_0 is the reference atmospheric pressure, 1.013×10^5 Pa. The first and last terms in the square brackets follow from the relationship between sound power level and sound pressure level in a diffuse field. The second term was introduced by Vorländer to compensate for an underestimation of the sound field using Sabine's equation. The third term is the Waterhouse correction. The fourth term accounts for atmospheric effects in the room and corrects the value to that measured with a characteristic specific acoustic impedance of 400 Pa·s/m.

2. Formulation using other field quantities

Two alternate quantities were considered in this study to obtain the sound power level of a source under test. One was the sound velocity level (SVL or L_u). The other was the total sound energy density level (SEDL or L_w). The sound velocity level is defined as ten times the base 10 logarithm of the ratio of the time-mean-square particle velocity of a given sound or vibration to the square of a specified reference particle velocity:[34]

$$L_u = 10 \log\left(\frac{u_{\mathrm{rms}}^2}{u_{\mathrm{ref}}^2}\right). \tag{12}$$

The reference value of u_{ref} has not been clearly standardized. Clause A.1 of ANSI S18-1989 notes that a reference particle velocity of 10 nanometers per second (10 nm/s) is used in ANSI S1.8-1969. This is in contrast with the 1 nm/s preferred by ISO 1683-1983.

Plane-wave conditions describe the relationship between particle velocity and acoustic pressure as

$$u = \frac{p}{\rho_0 c}. \tag{13}$$

It is reasonable then to assume that the reference velocity might be related to the reference pressure in the same way:

$$u_{\mathrm{ref}} = \frac{p_{\mathrm{ref}}}{\rho_0 c}. \tag{14}$$

However, if the characteristic impedance $\rho_0 c$ is estimated to be 400 Pa·s/m and p_{ref}=20 μPa, the reference velocity would be 50 nm/s. This value is much greater than either the ANSI or ISO suggestion, but its use is not uncommon.[35] In any case, if p_{ref} is considered to be the primary standard, a fixed u_{ref} may not remain sufficiently accurate, since ambient atmospheric conditions determine the value of $\rho_0 c$.

The total sound energy density level may be expressed as

$$L_w = 10 \log\left(\frac{\langle w \rangle_t}{w_{\mathrm{ref}}}\right), \tag{15}$$

where $\langle w \rangle_t$ is the time-averaged total energy density and w_{ref} is the reference energy density. The reference value may be determined from a summation of the squared pressure and particle velocity reference values, with appropriate weightings:

$$w_{\mathrm{ref}} = \frac{1}{2\rho_0 c^2} p_{\mathrm{ref}}^2 + \frac{\rho_0}{2} u_{\mathrm{ref}}^2. \tag{16}$$

For a plane wave, the sound pressure level, sound velocity level, and sound energy density level should all be equal, as long as the appropriate reference values are used. Thus, once L_u and L_w have been calculated, the sound power level can be determined from either of these values by inserting them

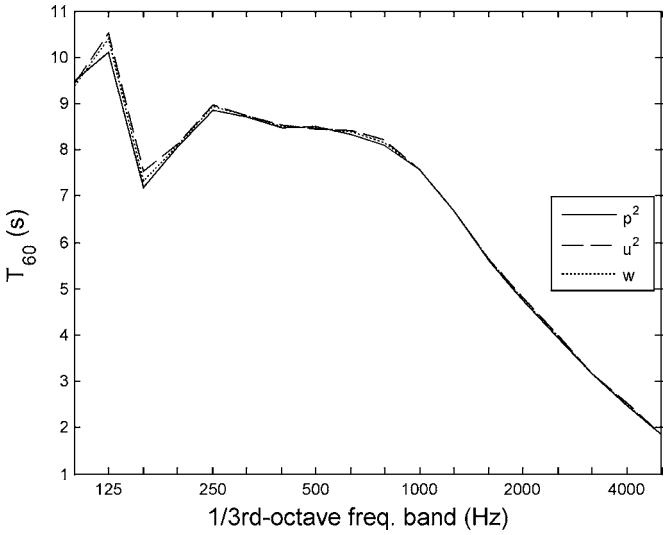

FIG. 2. Average T_{60} measurements based on squared pressure, squared velocity magnitude, and total energy density in the empty large chamber.

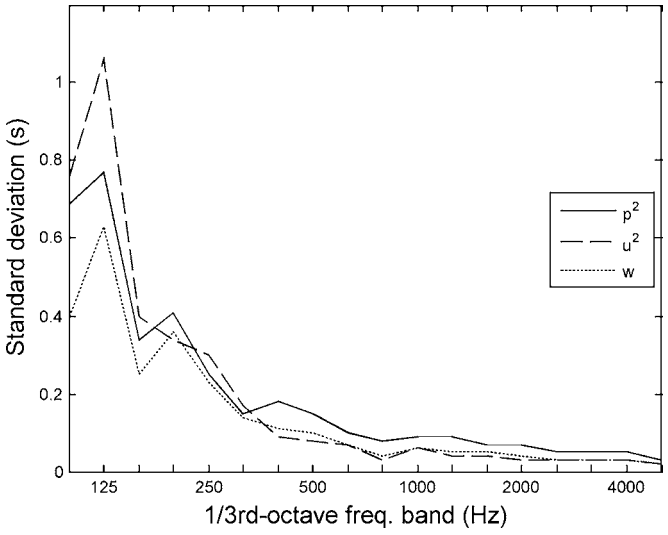

FIG. 3. Standard deviation of T_{60} measurements based on squared pressure, squared velocity magnitude, and total energy density in the empty large chamber.

in place of L_p in Eq. (11), with appropriate attention to correction terms. For this study, the Waterhouse correction term was chosen to be consistent when L_u was used because the value of the integrated interference pattern for kinetic energy density is the same as that for potential energy density.[5] When L_w was used, the number 8 in the denominator of the term was replaced by 4, for an assumed combination of the potential and kinetic energy density interference patterns. All other correction terms remained the same. The actual levels obtained in an enclosure are contingent upon the diffuseness of the sound field. Because the variation in the sound field is different for each quantity, the average sound levels will also differ for a given number of source-receiver locations.

III. EXPERIMENTAL RESULTS

A. Sound absorption

1. Reverberation time

For all T_{60} measurements, 12 source-receiver positions were used in each room for averaging, as required by the ISO 354 standard. The average T_{60} values were obtained from impulse responses based on squared pressure (p^2), squared particle velocity magnitude (u^2), and total energy density (w). They were then examined and compared. The probability of one measurement quantity outperforming the others (in terms of spatial uniformity) was obtained for various cases. These methods were repeated with and without the inclusion of test materials in the rooms.

Figure 2 shows the average T_{60} values and Fig. 3 shows their standard deviations for the empty large chamber using all 12 measurement positions. The average values agree, particularly at higher frequencies. Minor differences occur at 125 and 160 Hz. Total energy density w produces a notably lower standard deviation than p^2 at nearly all frequencies. Based on previous energy density studies, this was an anticipated result. At higher frequencies, u^2 significantly outperforms p^2. In fact, it appears to perform as well as, if not better than, w at these frequencies. This phenomenon was repeated in later observations. At lower frequencies, p^2 performs better than u^2.

To further investigate and visualize the performance of u^2 and w, probability tests were conducted to analyze the minimum number of positions required to achieve results as good as those for 12 standard measurement positions using p^2. All possible combinations of the data were evaluated as a function of the number of positions. The probability P that the standard deviation of T_{60} from r randomly chosen u^2 positions is lower than the standard deviation of T_{60} from all 12 p^2 positions is shown in Fig. 4. The probability for r randomly chosen w positions is shown in Fig. 5. Of the two quantities, w generally performs best over all frequencies. At

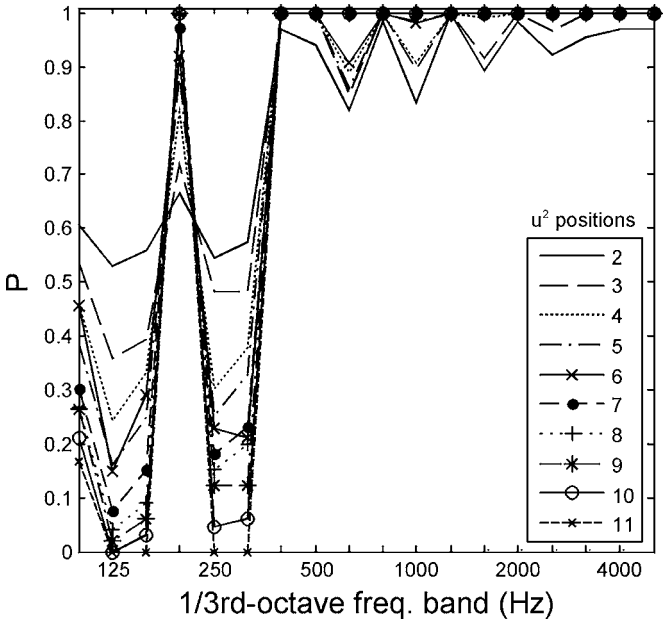

FIG. 4. Progressive probabilities that a given number of positions of squared velocity magnitude (u^2) outperform 12 squared pressure (p^2) measurements in the empty chamber.

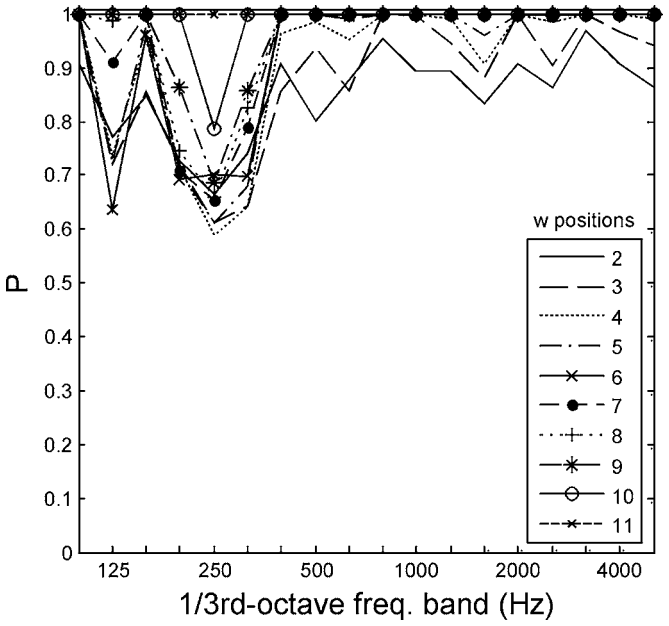

FIG. 5. Progressive probabilities that a given number of positions of total energy density (w) outperform 12 squared pressure (p^2) measurements in the empty chamber.

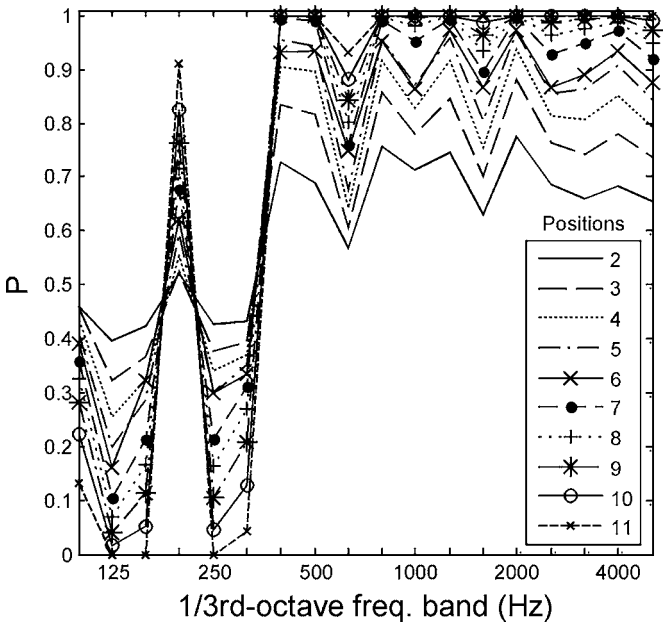

FIG. 6. Progressive probabilities of lower variation in u^2 vs. p^2 in the empty large chamber.

higher frequencies, six w positions ensure a lower standard deviation than the 12 p^2 positions. Standard deviation values for u^2 also do very well at higher frequencies; seven positions are enough to outperform the p^2 positions. In both cases, a transition to lower probabilities is apparent below the Schroeder frequency of 410 Hz. While the number of measurement positions needed below the Schroeder frequency becomes greater, one generally observes that fewer w positions are necessary than either p^2 or u^2 positions. Above the Schroeder frequency, either w or u^2 leads to fewer measurement positions.

For yet another point of view, an additional comparison was made by evaluating the probability that any number of randomly chosen positions for one quantity led to a lower variation than the same number of randomly chosen positions for any other quantity. Two relationships were plotted: u^2 vs. p^2, and w versus p^2. The results are given in Figs. 6 and 7, respectively. The probability that variation is lower for either u^2 or w increases with the number of positions. To see if the performance of u^2 versus w was indeed significant, an F test of unequal variances was used.[36] The test revealed that for a 95% confidence level, the standard deviation values were statistically equal, except at 100 Hz, where that for w was smaller. This phenomenon was further investigated analytically, as will be discussed in the next section.

The T_{60} results were also compared when absorptive materials were present in the room. The measurements and comparisons were likewise repeated for the small chamber. As reported in Ref. 30, the results for the various averages and standard deviations were similar to those discussed above, especially at frequencies above the Schroeder frequency.

2. Absorption coefficients

The sound absorption coefficients for the test samples were calculated according to the procedures outlined in ISO 354. The calculations were based on the impulse responses from the 12 source-receiver positions. From the T_{60} results, half the w positions were sufficient to obtain results comparable with the p^2 results above the Schroeder frequency. Six u^2 and w positions were thus randomly chosen and compared to all 12 p^2 positions for calculation of the absorption coefficients. Although this number was not sufficient for the entire measurement bandwidth, it showed that the results are generally similar to those of the conventional measurements. Figures 8 and 9 show the absorption coefficient (α_s) results obtained from the two chambers. The ±10% accuracy window described in ISO 9613-1 was calculated based on the atmospheric absorption α obtained for the squared-pressure

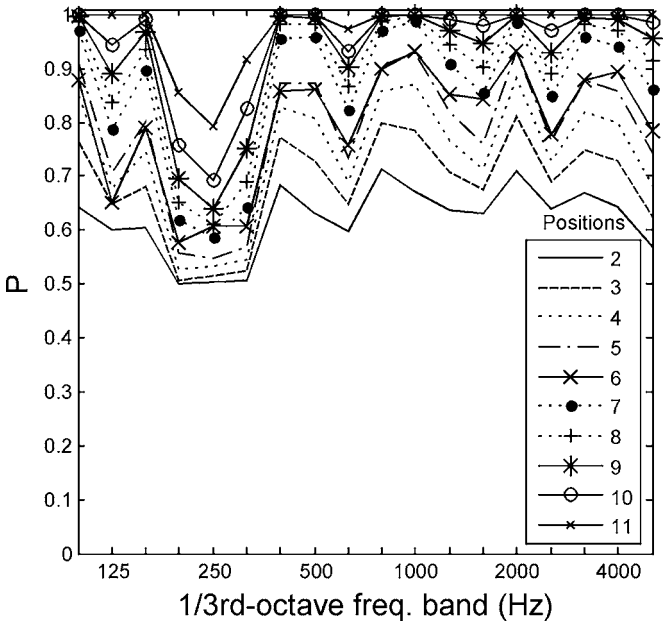

FIG. 7. Progressive probabilities of lower variation in w vs. p^2 in the empty large chamber.

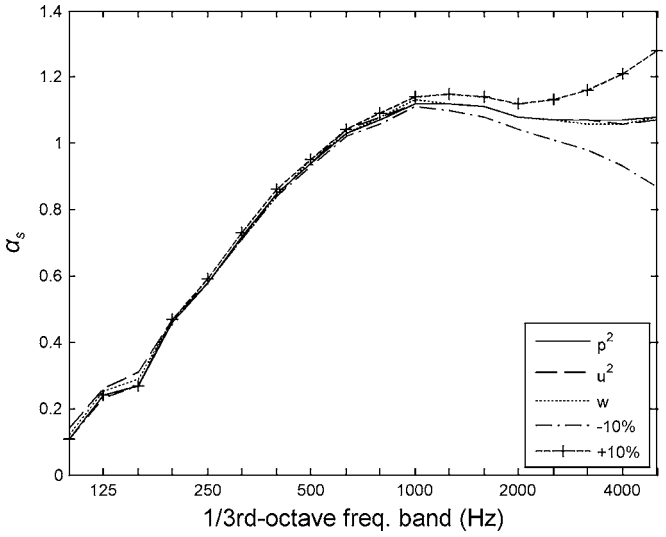

FIG. 8. Measured absorption coefficients of 5 cm thick fiberglass insulation in the large chamber. The three curves are obtained from 12 p^2 positions and from 6 random u^2 and w positions. The accuracy limits due to calculation of the air attenuation coefficient are also plotted.

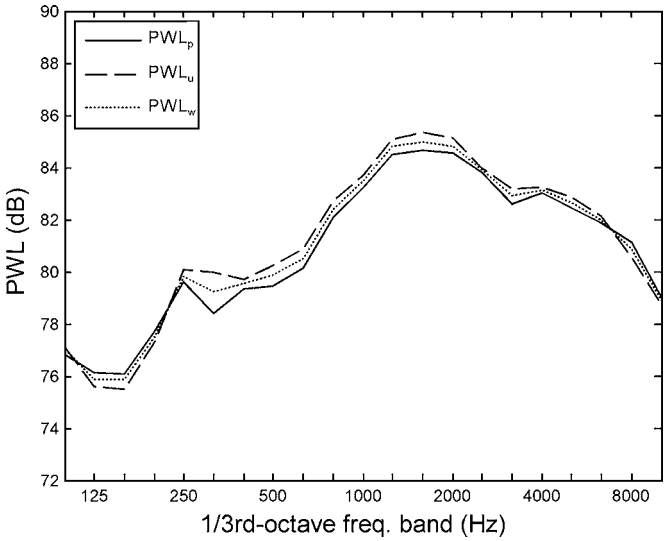

FIG. 10. Sound power levels (PWL) for a reference sound source at one position in the large chamber. The three curves labeled PWL_p, PWL_u, and PWL_w were obtained from six spatially averaged SPL, SVL, and SEDL measurements, respectively.

measurements. (In other words, the window is calculated from the values 1.1α and 0.9α at each frequency.)

These plots demonstrate that the results are very similar for a given room, no matter which measurement quantity is used. Because of the smaller spatial variations of T_{60} for both u^2 and w, fewer measurement positions can be used to obtain the absorption coefficients. In this case, the number of positions was reduced by one-half. A comparison of the measurements from the two chambers reveals that they are quite similar, although some differences do exist.

B. Sound power

A Brüel and Kjær 4204 reference sound source was used for all sound power measurements. Six receiver positions and one source position were chosen in the large chamber, the minimum required by the ISO 3741 standard. Three receiver positions and two source positions were chosen in the small chamber, due to its smaller working area. The spatially averaged SPL, SVL, and SEDL values were obtained and used to determine the sound power of the source. Figure 10 shows the results from the large chamber and Fig. 11 shows the corresponding standard deviations. Similar results are given for the small chamber in Figs. 12 and 13 (note that Fig. 13 uses a larger vertical scale than Fig. 11). The allowed standard deviations of sound pressure levels for the measured field points (see ISO 3741) are included in the standard deviation plots. Where the measured standard deviations exceed the limits, more source and/or receiver positions become necessary.

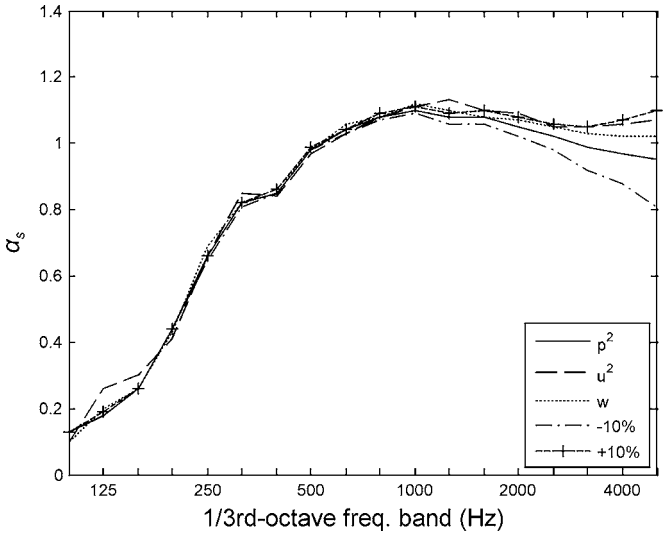

FIG. 9. Measured absorption coefficients of 5 cm thick fiberglass insulation in the small chamber. The three curves are obtained from 12 p^2 positions and from 6 random u^2 and w positions. The accuracy limits due to calculation of the air attenuation coefficient are also plotted.

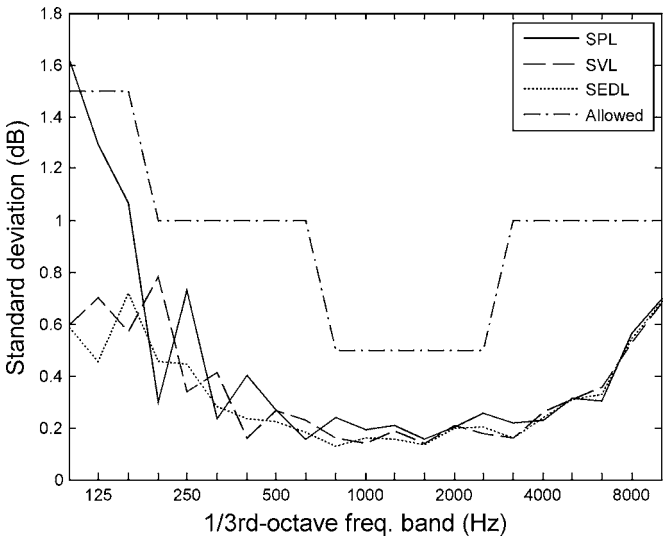

FIG. 11. Measured and allowed standard deviations of sampled field quantities used to assess the sound power produced by a source in the large chamber. Standard deviation values exceeding the allowed limits require additional source and/or receiver positions. The SVL and SEDL measurements are shown to extend the usable low-frequency range of the chamber without the addition of low-frequency absorption.

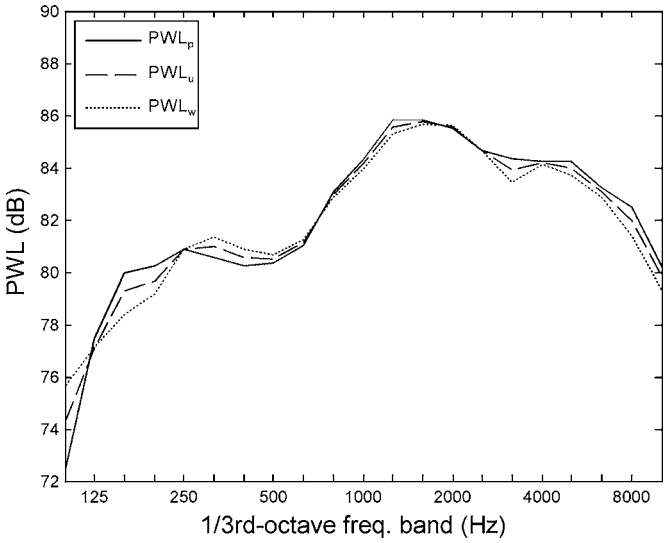

FIG. 12. Sound power levels (PWL) for a reference source in the small chamber. The three curves labeled PWL_p, PWL_u, and PWL_w were obtained from six spatially averaged SPL, SVL, and SEDL measurements, respectively, which involved two source positions.

The sound power levels obtained from the SPL, SVL, and SEDL measurements are similar within each chamber, while the results from one chamber vary slightly from those of the other. In the large chamber, the standard deviation of the SPL values barely exceeds the allowed deviation at the lowest frequencies. As suggested before, this problem is due to low modal overlap and would likely be corrected with the addition of low-frequency absorbers. Standard deviation values determined from SVL and SEDL perform much better at these lower frequencies. This suggests that the addition of low-frequency absorbers may not be necessary if sound power is determined via particle velocity magnitude or total energy density.

As expected, the results for the small chamber show that the standard deviation of the SPL is very poor at lower frequencies. The standard deviation of the SVL is better, but it still exceeds the allowed value in the 125-Hz octave band. However, the standard deviation of the SEDL is well within allowed limits at all frequencies, including the problematic lower frequencies. This suggests that total energy density measurements could be used to better estimate low-frequency sound power of sources in smaller rooms with modal overlap that is typically considered inadequate.

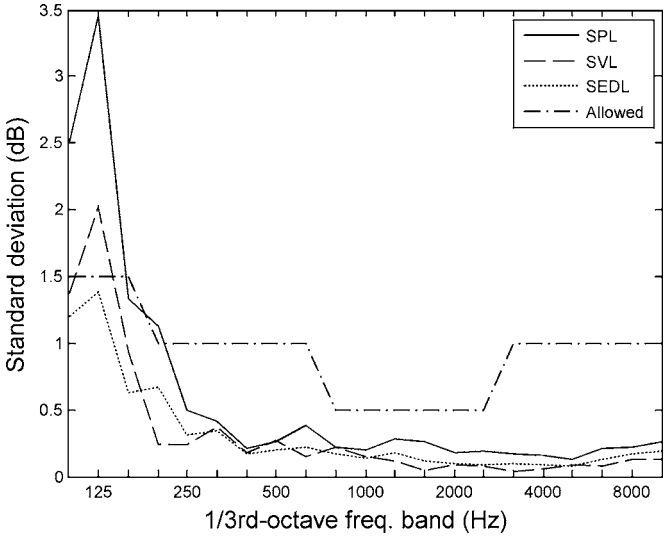

FIG. 13. Measured and allowed standard deviations of sampled field quantities used to assess the sound power produced by a source in the small chamber. Standard deviation values exceeding the allowed limits require additional source and/or receiver positions. The SEDL measurements are shown to extend the usable low-frequency range of the chamber.

IV. ADDITIONAL DISCUSSION

A. Theoretical and numerical modeling

Simple theoretical and numerical models were developed to simulate the acoustical characteristics of the large chamber and enhance understanding of the experimental measurement results.[30] The room was modeled as an ideal rectangular enclosure with dimensions $5\text{m} \times 6\text{m} \times 7\text{m}$, large wall impedance, and spectrally uniform damping. The frequency-dependent complex acoustic pressure amplitude $\hat{p}(x,y,z)$ was calculated at points in the enclosure due to a point source at a fixed position using a familiar eigenfunction expansion.[37] The Cartesian components of the frequency-dependent particle velocity $\hat{\mathbf{u}}(x,y,z)$ were determined from the expansion by applying Euler's equation for each dimension in its time-harmonic form. The time-averaged potential energy density at each point was subsequently obtained using the expression

$$\langle w_p(x,y,z)\rangle_t = \frac{1}{4\rho_0 c^2}\hat{p}(x,y,z)\hat{p}^*(x,y,z) = \frac{1}{4\rho_0 c^2}|\hat{p}(x,y,z)|^2 \tag{17}$$

and the time-averaged kinetic energy density was obtained using the expression

$$\begin{aligned}\langle w_k(x,y,z)\rangle_t &= \frac{\rho_0}{4}\hat{\mathbf{u}}(x,y,z)\cdot\hat{\mathbf{u}}^*(x,y,z)\\ &= \frac{\rho_0}{4}[|\hat{u}_x(x,y,z)|^2 + |\hat{u}_y(x,y,z)|^2\\ &\quad + |\hat{u}_z(x,y,z)|^2].\end{aligned} \tag{18}$$

The time-averaged total energy density was then calculated as the sum of the potential and kinetic energy density components.

Thousands of receiver locations were required in the calculations to adequately describe the spatial variation of the three-dimensional field. While it would have been difficult and time consuming to perform actual measurements at such high resolution throughout the chamber volume, it was relatively simple to simulate them using the computer model. An effort was made to include a sufficient number of modes in the calculations. For an analysis through the 5-kHz one-third-octave band, up to 7.5 million modes were involved. An absorption coefficient of 0.02 was chosen for all room surfaces, at all frequencies of interest. This value produced a T_{60} value of 7.9 s, a uniform modal bandwidth of 0.27 Hz,[37] and a Schroeder frequency of 388 Hz. The modal damping factor δ_N also followed from the coefficient.[38]

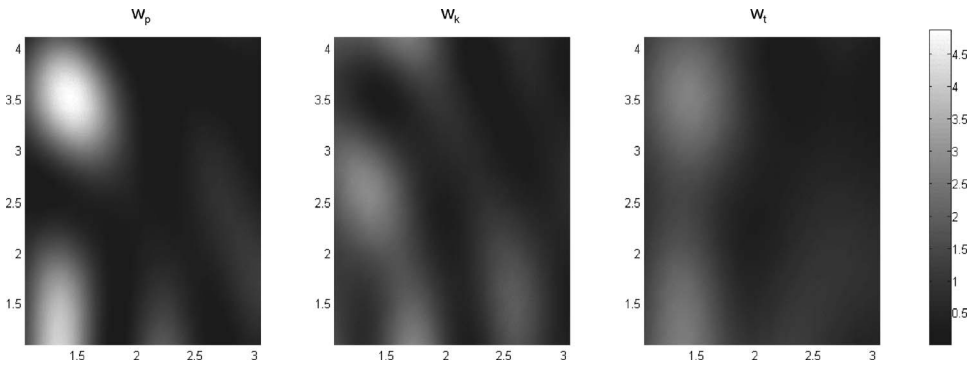

FIG. 14. Mapped potential, kinetic, and total energy density fields for the $z=3$ m plane of the modeled large chamber, in the 125-Hz one-third-octave band. For this example, the source was positioned in the lower corner of the chamber at $(x,y,z)=(0,0,0)$.

The spatial variation was calculated for the one-third-octave bands between 100 and 5000 Hz. The calculations were obtained by summing the contributions of 1-Hz bins within each band. To reduce computation time, only the modes that fell within nearly ten times the modal bandwidth at each frequency bin were used, since those outside this range contributed much less significantly to the results. The source strength of the point source was set to unity. In the case illustrated here, the source was positioned in a lower corner of the room ($x_0=0$ m, $y_0=0$ m, $z_0=0$ m). Field quantities were calculated at 0.1-m increments in x, y, and z, beginning 1 m away from each wall, and 2 m away from the source, yielding 52, 111 positions in total. The distances from the walls and source were chosen for consistency with the practices outlined in ISO 3741.

Pertinent field values for each plane in z were saved to separate Matlab files for later extraction and analysis. Each file included pressure, particle velocity magnitude, potential energy density, kinetic energy density, and total energy density. The data were eventually grouped for two cases: variation over the entire volume and variation over each plane in z. Given the fixed room properties, the variables affecting the outcome included the source position, receiver plane, and frequency. To equitably compare the variation for each field quantity, the standard deviation was calculated after normalizing the data by its mean value. This resulted in a new average value of 1 and a dimensionless standard deviation. This method of normalization was chosen because measurements deal with average values.

Figure 14 shows the normalized potential, kinetic, and total energy density fields for the 125-Hz one-third-octave band and the $z=3$ m plane of the model. Similar results could be presented for any plane in the room. One notes from the figure that the maxima of the potential energy density field often fall near the minima of the kinetic energy density field and vice versa. Figure 15 shows the frequency-dependent standard deviations of the normalized fields throughout the entire volume, with the source in the corner as indicated above. Just as for the experimental sound power measurements for the large chamber, both kinetic and total energy density outperformed potential energy density in terms of spatial uniformity. The performances of kinetic and total energy density are quite similar. At higher frequencies, the results agree reasonably well with the predictions given by Jacobsen.[7] An F test for unequal variances revealed that in most cases, for a 99% confidence level, the standard deviations of kinetic and total energy densities are statistically equal.

B. Uncertainty errors due to atmospheric conditions

As explained earlier, the uncertainties in reverberation chamber measurements come from many sources. Some involve the atmospheric conditions in the rooms. For the acoustical measurements reported in this paper, temperature, relative humidity, and barometric pressure were regularly evaluated. The respective values had the following margins of error for the measurement instrument used: ±1 °C, ±7% RH, and ±700 Pa. All three values were used to obtain the air attenuation coefficient α. The coefficient is based on a theoretical calculation of the relaxation frequencies of nitrogen and oxygen, as detailed in ISO 9613, with accuracy to ±10%. Of the three atmospheric values, temperature most strongly affects the speed of sound. An uncertainty of ±1 °C results in a variation of ±0.6 m/s.

The uncertainty present in the air attenuation coefficient has a considerable effect on the equivalent absorption area at frequencies above 1 kHz. For example, the error value of α at 5 kHz for the fiberglass insulation absorption in the large chamber is ±0.21, according to the 10% accuracy limits. In comparison, the error value of α due to an uncertainty of

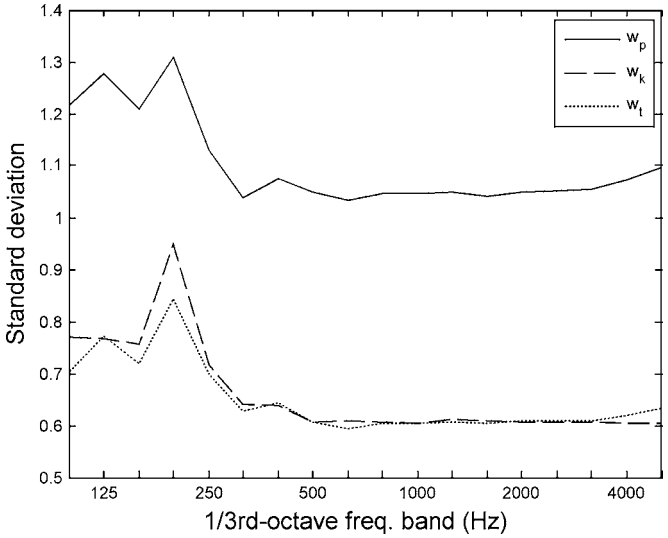

FIG. 15. Standard deviation curves for the normalized potential, kinetic, and total energy density throughout the modeled room volume.

±1 °C alone is ±0.08. Accordingly, it appears that the uncertainty from the measured atmospheric values is not as significant as that inherent in the standard itself. However, the uncertainty effects are further accentuated in the calculation of energy density, which uses both ρ_0 and c. The uncertainties of the three atmospheric values result in an overall uncertainty of ±0.013 kg/m^3 for ρ_0. Thus, the energy density impulse response might introduce additional errors in the measured T_{60}, an issue absent in the squared-pressure impulse response. This also affects the sound power level obtained from the SEDL by ±0.1 dB. Are these effects negligible? Since T_{60}, absorption coefficients, and sound power are all based on spatially averaged values, some effects may be averaged out. Furthermore, measurement results are often rounded to the nearest tenth or hundredth value.[19,20] Other errors exist from theoretical assumptions alone. The reproducibility of reverberation chamber measurements also continues to be investigated.[20] The combined uncertainties from several factors in these measurements are likely to have a greater effect than the uncertainties present in the ρ_0 and c values alone.

V. SUMMARY AND CONCLUSIONS

This work has demonstrated that total acoustic energy density may be beneficially used in reverberation chamber measurements. The principal characteristic that makes it more attractive than squared pressure or potential energy density is its greater spatial uniformity over an enclosed sound field. Reverberation chamber measurements suffer from uncertainties associated with diffuse field approximations. Total energy density was expected to reduce measurement error or simplify measurement processes by requiring fewer measurement positions.

The work has specifically introduced methods of measuring sound absorption and sound power using total energy density. An energy density impulse response can be obtained by combining the squared-pressure impulse response and a squared-velocity-magnitude impulse response with appropriate weightings. The resulting response can then be used to determine reverberation time and sound absorption. The sound power level of a source can also be calculated in a reverberation chamber using the total sound energy density level (SEDL). Several procedures for implementing these measurements and the implications of atmospheric variable errors have been described in the paper.

Results from T_{60} measurements in two reverberation chambers show greater spatial uniformity of decay using the total energy density impulse response. In a large qualified chamber, the variation was roughly one-half that of the squared-pressure impulse response. The results suggest that fewer source-receiver positions are necessary to obtain an adequate sampling of the sound field. They also suggest that low-frequency T_{60} measurements are more consistent when using the energy density method. Similar results were found in a small reverberation chamber. The benefits automatically extend to the calculation of sound absorption values. Results from both chambers showed similar values for measured absorption coefficients that were comparable to those obtained from the standard squared-pressure method in the qualified chamber.

The sound power level of a reference sound source was also measured using both total energy density and squared pressure. Under steady-state conditions, total energy density was shown to have greater spatial uniformity than squared pressure in both chambers. With squared pressure, one source position, and six receiver positions, the large chamber failed to meet ISO requirements for variation in the 100-Hz third-octave band. This was in part because it was not fitted with low-frequency absorption. Nevertheless, it did meet the requirements when using total energy density and the same measurement positions. The variation of the latter was significantly lower than the maximum allowable variation at all frequencies of interest. This result was encouraging because it suggested that the low-frequency absorption and more source and receiver positions would not necessarily be required. It could also limit the need to reconfigure the chamber for different types of measurements. Results in the small chamber showed that the standard deviation values obtained from total energy density at low frequencies also met the ISO requirements, despite the fact that the room had a much smaller volume than required. Inclusion of the factors ρ_0 and c adds some uncertainty to SEDL measurements when atmospheric variables are not completely certain.

The investigation also revealed that the squared vector magnitude of the particle velocity often resulted in much smaller variations than squared pressure for both T_{60} values and sound levels. The degree of variation was quite similar to that of total energy density, especially at higher frequencies. In some cases, it was slightly better than that of total energy density. However, tests using both experimental and numerical data revealed that this observation was statistically insignificant. While the particle velocity measurements suggested that kinetic energy density alone could provide viable improvements to reverberation chamber measurements, it was found to be less consistent than total energy density over full measurement bandwidths.

This work has thus shown that total energy density can be used to successfully measure sound absorption and sound power in reverberation chambers with fewer measurement positions than required for squared pressure. It has also demonstrated that a fixed number of total energy density measurements may extend the usable low-frequency ranges of chambers with different volumes and limited low-frequency absorption (although this does not guarantee assumed diffuseness of their fields).

The investigation has suggested several topics that merit further investigation. For example, the study used a small number of discrete measurement positions according to ISO 354 and 3741. A thorough investigation of the sound field in a small enclosure would be beneficial to determine whether more accurate low-frequency measurements can be obtained in such a space by sampling the total energy density field with many more measurement positions than typically required in the standards. The impact of diffusers on the energy density methods should also be explored. The study was limited to sound absorption and sound power measurements.

The benefits of kinetic and total energy densities should also be explored for other types of reverberation chamber measurements, including sound transmission and sound scattering measurements. The authors encourage additional research in these areas.

ACKNOWLEDGMENTS

This research was sponsored by the National Science Foundation (NSF). The authors also thank Microflown Technologies and Larson Davis (PCB Piezotronics) for the use of key experimental devices.

[1]J. Tichy and P. Baade, "Effect of rotating diffusers and sampling techniques on sound-pressure averaging in reverberation rooms," J. Acoust. Soc. Am. **56**, 137–143 (1974).
[2]R. K. Cook and P. A. Schade, "New method for measurement of the total energy density of sound waves," Proceedings of Inter-Noise 74, Washington DC, 1974, pp. 101–106.
[3]L. W. Sepmeyer and B. E. Walker, "Progress report on measurement of acoustic energy density in enclosed spaces," J. Acoust. Soc. Am. **55**, S12(A) (1974).
[4]R. V. Waterhouse and R. K. Cook, "Diffuse sound fields: Eigenmode and free-wave models," J. Acoust. Soc. Am. **59**, 576–581 (1976).
[5]R. V. Waterhouse, "Interference patterns in reverberant sound fields," J. Acoust. Soc. Am. **27**, 247–258 (1955).
[6]R. V. Waterhouse and R. K. Cook, "Interference patterns in reverberant sound fields. II," J. Acoust. Soc. Am. **37**, 424–428 (1965).
[7]F. Jacobsen, "The diffuse sound field: Statistical considerations concerning the reverberant field in the steady state," The Acoustics Laboratory, Technical University of Denmark, Report No. 27 (1979).
[8]J. A. Moryl, "A study of acoustic energy density in a reverberation room," M.S. thesis, The University of Texas at Austin, Austin, TX, 1987.
[9]J. A. Moryl and E. L. Hixson, "A total acoustic energy density sensor with applications to energy density measurement in a reverberation room," Proceedings of Inter-Noise 87, Beijing, China, 1987, Vol. II, pp. 1195–1198.
[10]J. Parkins, S. Sommerfeldt, and J. Tichy, "Narrowband and broadband active control in an enclosure using the acoustic energy density," J. Acoust. Soc. Am. **108**, 192–203 (2000).
[11]D. Bonsi, D. Gonzalez, and D. Stanzial, "Quadraphonic impulse responses for acoustic enhancement of audio tracks: measurement and analysis," Forum Acusticum (2005), pp. 335–340.
[12]I. Wolff and F. Massa, "Use of pressure gradient microphones for acoustical measurements," J. Acoust. Soc. Am. **4**, 217–234 (1933).
[13]F. Fahy, "Measurement of acoustic intensity using the cross-spectral density of two microphone signals," J. Acoust. Soc. Am. **62**, 1057–1059 (1977).
[14]F. J. Fahy, *Sound Intensity*, 2nd ed. (E & FN Spon, London, 1995).
[15]J. Ghan, "Expression for the estimation of time-averaged acoustic energy density using the two-microphone method (L)," J. Acoust. Soc. Am. **113**, 2404–2407 (2003).
[16]G. W. Elko, "An acoustic vector-field probe with calculable obstacle bias," Proc. Noise-Con **91**(7), 525–532 (1991).
[17]H-E. de Bree, "An overview of Microflown technologies," Acta Acust. **31**, 91–94 (2003).
[18]R. Raangs, Exploring the use of the Microflown, Ph.D. dissertation, University of Twente, 2005.
[19]ISO 3741:1999(E), "Acoustics—Determination of sound power levels of noise sources using sound pressure—Precision methods for reverberation rooms" (International Organization for Standardization, Geneva, 1999).
[20]ISO 354:2003, "Acoustics—Measurement of sound absorption in a reverberation room" (International Organization for Standardization, Geneva, 2003).
[21]A. Schaffner, "Accurate estimation of the mean sound pressure level in enclosures," J. Acoust. Soc. Am. **106**(2), 823–827 (1999).
[22]M. Vorländer, "Revised relation between the sound power and the average sound pressure level in rooms and the consequences for acoustic measurements," Acustica **81**, 332–343 (1995).
[23]R. V. Waterhouse, "Statistical properties of reverberant sound fields," J. Acoust. Soc. Am. **43**, 1436–1444 (1968).
[24]D. Lubman, "Fluctuations of sound with position in a reverberant room," J. Acoust. Soc. Am. **44**, 1491–1502 (1968).
[25]J. L. Davy, I. P. Dunn, and P. Dubout, "The Variance of Decay Rates in Reverberation Rooms," Acustica **43**, 12–25 (1979).
[26]C. Eyring, "Reverberation time in dead rooms," J. Acoust. Soc. Am. **1**, 217–214 (1930).
[27]M. Hodgson, "On measures to increase sound-field diffuseness and the applicability of diffuse-field theory," J. Acoust. Soc. Am. **95**(6), 3651–3654 (1994).
[28]K. H. Kutruff, "Sound decay in reverberation chambers with diffusing elements," J. Acoust. Soc. Am. **69**, 1716–1723 (1981).
[29]M. Schroeder, "New method of measuring reverberation time," J. Acoust. Soc. Am. **37**, 409–412 (1965).
[30]D. Nutter, "Sound absorption and sound power measurements in reverberation chambers using energy density methods," M.S. thesis, Brigham Young University, 2006.
[31]ISO 9613-1:1993(E), "Acoustics—Attenuation of sound during propagation outdoors—Part 1: Calculation of the absorption of sound by the atmosphere" (International Organization for Standardization, Geneva, 1993).
[32]A. Pierce, *Acoustics, An Introduction to Its Physical Principles and Applications* (Acoustical Society of America, Melville, NY, 1989).
[33]G. Mange, "The effect of mean free path on reverberation room measurement of absorption and absorption coefficients," Noise Control Eng. J. **53**(6), 268–270 (2005).
[34]ANSI S1.1-1994, "Acoustical terminology" (American National Standards Institute, New York, 1994).
[35]D. Stanzial, D. Bonsi, and N. Prodi, "Measurement of new energetic parameters for the objective characterization of an opera house," J. Sound Vib. **232**, 192–211 (2000).
[36]G. Keller, *Applied Statistics with Microsoft® Excel* (Duxbury, Pacific Grove, CA, 2001).
[37]H. Kuttruff, *Room Acoustics*, 4th ed. (Spon, New York, 2000).
[38]P. A. Nelson and S. J. Elliott, *Active Control of Sound* (Academic, London, 1992).